electronics

Article

A Novel Pull-Up Active-Clamping Wireless Charging Circuit with Low Cost and Voltage Stress

Bo Pan [1], Houji Li [1], Yong Wang [1] and Deshu Zhang [2,*]

[1] Department of Electrical Engineering, Shanghai Jiao Tong University, Shanghai 200240, China; panbost@163.com (B.P.); lihoushen@sjtu.edu.cn (H.L.); wangyong75@sjtu.edu.cn (Y.W.)
[2] Chuzhou Polytechnic, Chuzhou 239000, China
* Correspondence: zhangdeshu@chzc.edu.cn

Abstract: The traditional single-switch circuit has the advantages of fewer components, no shoot-through problems, and suitability for high-frequency wireless charging applications. However, because of the high voltage stress of the switch, the bulky inductor, and the narrow soft-switching range, its power and applications have some limitations. To relieve this problem, this paper proposes a pull-up active-clamping circuit, which not only offers a low component count with no bulky inductors, but also greatly reduces the switch voltage stress. In addition, a wide range of soft switching can be achieved by designing a primary-side compensation capacitor. A detailed parametric design method is given and compared with existing circuits from the aspects of switch voltage stress, component count, efficiency, cost, and so on. Finally, a 1 MHz, 180 W active-clamping wireless charging system is built to verify the proposed circuit and design method.

Keywords: pull-up active-clamping circuit; wireless charging; switch voltage stress; zero-voltage switching

check for updates

Citation: Pan, B.; Li, H.; Wang, Y.; Zhang, D. A Novel Pull-Up Active-Clamping Wireless Charging Circuit with Low Cost and Voltage Stress. *Electronics* **2023**, *12*, 2834. https://doi.org/10.3390/electronics12132834

Academic Editor: Fabio Corti

Received: 14 May 2023
Revised: 22 June 2023
Accepted: 23 June 2023
Published: 27 June 2023

1. Introduction

Wireless power transfer (WPT), which has great potential for development, has made the transmission methods and application scenarios of electricity more diverse and extensive. Wireless power transfer technology can transmit electrical energy without physical connections by using magnetic fields, electric fields, microwaves, and lasers, etc. Currently, WPT technology is widely used in electric vehicle charging, tailless kitchen power, portable devices, implantable medical devices, aerospace, rail transportation, and other fields. Since there is no physical connection, WPT technology has the advantages of convenience and flexibility, safety and reliability, and applicability to extreme situations compared to plug-in wired electrical energy transmission methods.

At present, the main circuit of wireless charging systems usually employs full bridge-voltage-type topology, a half-bridge topology, and a single-switch topology similar to a Class E circuit [1]. The bridge circuit generally requires more switch counts, complex gate-driving schemes, and may sometimes cause shoot-through issues. In addition, bridge circuits typically have high dv/dt drain source voltages, and significant dv/dt stress can decrease the life of insulation materials as time increases [2]. In addition, due to the need for complementary conduction in bridge circuits, it is not as reliable as a single-switch circuit in situations with high switching frequency.

Single switch circuits, like Class E, have the advantages of a smaller number of components, no shoot-through issues, a simple drive method, high reliability, and suitability for high-frequency wireless charging applications [3–5]. But, the switching voltage stress of a single switch circuit could be as high as three to four times the input voltage, limiting its output power and applications [6]. In addition, for infinite Class E circuits, a large inductor at the front is generally required; for finite Class E circuits, the inductor at the front is an AC inductor, both of which make the system power density decrease and circuit losses increase. Moreover, traditional single-switch circuits such as Class E also have a narrow soft-switching range, resonant waveform unipolar irregularity, low transmission power, bulky inductor, and other defects [7,8]. In [9], a Class EF circuit is proposed, in which an LC resonant tank is added to the traditional Class E circuit to reduce switching voltage stress. The authors in [10] proposed a single-switch circuit for medium-power wireless charging, which eliminates the requirement for a bulky input inductor within the main circuit. But, the Class EF circuit needs more resonant devices and DC inductors, reducing system power density, and the single-switch circuit also has high switch voltage stress.

Therefore, the design of a circuit with low switch voltage stress and low component count is important for small- and medium-power wireless charging applications. A novel pull-up active-clamping circuit is proposed in this paper for a low-cost and compact-size wireless charging system. The proposed circuit has a low component count, low switch voltage stress, and no bulky inductor, resulting in high reliability and small volume. Moreover, the circuit does not require an accurate complementary drive design; the duty cycle of the auxiliary switch can be constant, and the output power can be controlled by changing the duty cycle of the main switch. In addition, both the main switch and the auxiliary switch of the proposed pull-up active-clamping circuit can achieve zero turn-on voltage and low dv/dt waveform in a wide load resistance range. Compared with the pull-down active-clamping circuit, the proposed pull-up active-clamping circuit reduces the voltage of the clamping capacitor without changing its characteristics. This paper presents a detailed modal analysis of the circuit, analyzes the voltage stress of switches and parameters, designs the method, and gives a detailed design discussion and the formulas to optimize the compensation capacitors. The proposed pull-up active-clamping circuit is also compared with existing circuits on the basis of switching voltage stress, the number of components, system efficiency, and cost to verify the feasibility of the proposed circuit and parameter design method.

2. The Pull-Up Active-Clamping Wireless Charging System

2.1. Main Circuit

A traditional single-switch circuit, like the Class E circuit, is shown in Figure 1. This circuit typically demands a large input inductor L_1 and a high switch voltage Q, resulting in low power density and low output power. In order to reduce the use of passive devices, especially inductors, and reduce the switch voltage stress, this paper proposes a pull-up active-clamping circuit for wireless charging applications, as shown in Figure 2. For ease of analysis, the input power supply is represented by a constant voltage source. C_p is a primary-side compensation capacitor, parallel with L_p, Q_1 is the main switch, and Q_2 is the auxiliary switch. L_p and L_s are the transmitter coil and receiving coil, respectively. C_s is the secondary-side compensation capacitor, in series with L_s. C_p and C_s constitute the typical WPT system with parallel-series (PS) compensation, respectively. A branch composed of switch Q_2 and clamp capacitor C_c or C_{c2}, representing pull-down or pull-up, is added to the active-clamp circuit. Subsequently, the pull-up active clamp is used as an example for analysis.

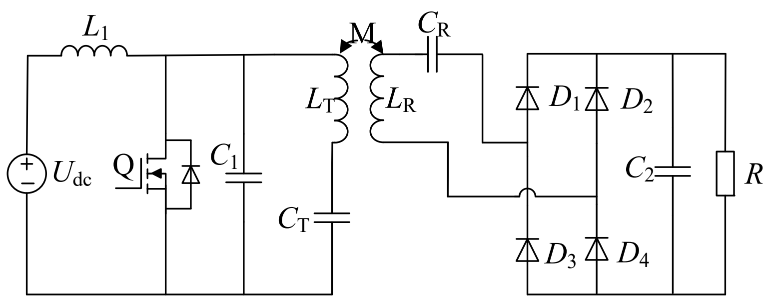

Figure 1. Class E circuit for wireless charging.

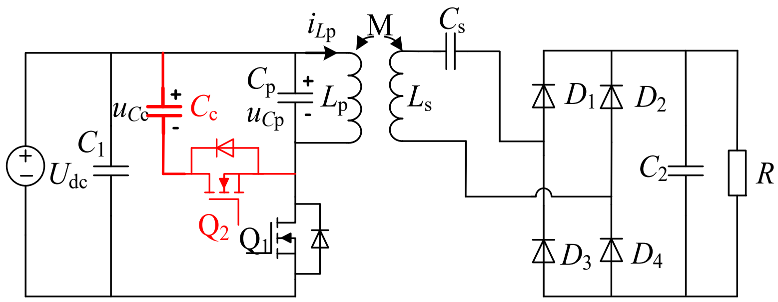

Figure 2. Proposed pull-up active-clamping circuit for wireless charging.

2.2. Operation Principle of the Pull-Up Active-Clamping Circuit

Figure 3 shows the operation waveform of the proposed circuit via simulation. Here, u_{gs1} represents the driving waveform of the main switch Q_1, u_{gs2} represents the driving waveform of Q_2, u_{ds1} represents the drain source waveform of Q_1, u_{ds2} represents the drain source waveform of Q_2, u_{Cp} represents the voltage of the primary-side compensation capacitor, i_{Lp} represents the current of the transmitting coil, and u_{Cc} represents the voltage of the active-clamp capacitor. For the proposed pull-up active-clamping wireless charging circuit, the main switch and the auxiliary switch can be turned on at any duty cycle only to ensure a certain dead time, without the need for the complementary conduction of two switches like the half-bridge circuit. In addition, the larger the duty cycle of the main switch, the greater the output power. The auxiliary switch can conduct at any time during the process of turning off the main switch. In addition, the smaller the duty cycle of the auxiliary switch, the greater the voltage stress difference between the main switch and the auxiliary switch.

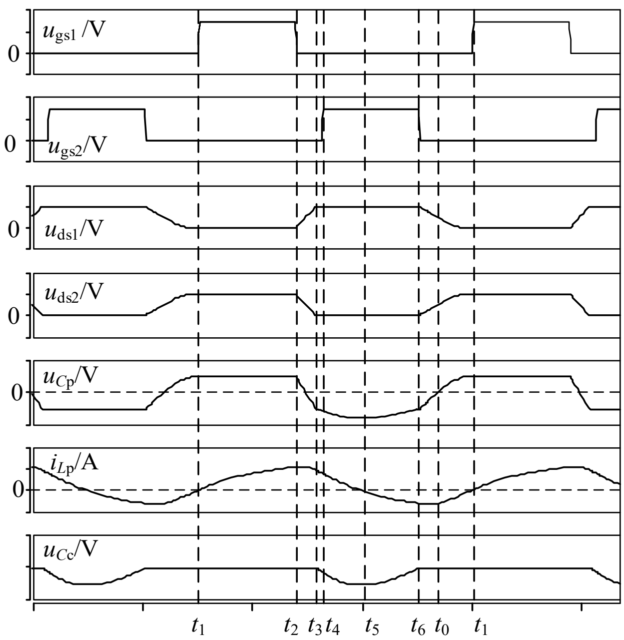

Figure 3. Operation waveforms of the circuit.

Figure 4 illustrates the six operating modes of the circuit. To facilitate the analysis, the following assumptions are presented.

(1) There are no parasitic inductances or parasitic capacitors.
(2) Switches and their body diodes are ideal.
(3) The internal resistance of other devices is ignored, except for the internal resistance of the transmitting and receiving coils.

All switches are on the primary side. Equivalent the secondary side circuit to the primary side for analysis.

Mode 1 [t_0 ~ t_1]: In Mode 1, the body diode of the main switch Q_1 is working in conduction to provide a reverse current path of i_{Lp}, so that the main switch Q_1 can achieve ZVS at time t_1, and in this period, the current of i_{Lp} decreases linearly to zero.

Mode 2 [t_1 ~ t_2]: In Mode 2, the main switch is turned on with the character of ZVS, the voltage of the primary-side compensation capacitor C_p is limited to the value of U_{dc}, the current i_{Lp} increases linearly to I_{Lp}, and the voltage stress of the auxiliary switch Q_2 is equal to U_{dc} + u_{Cc} (t_5).

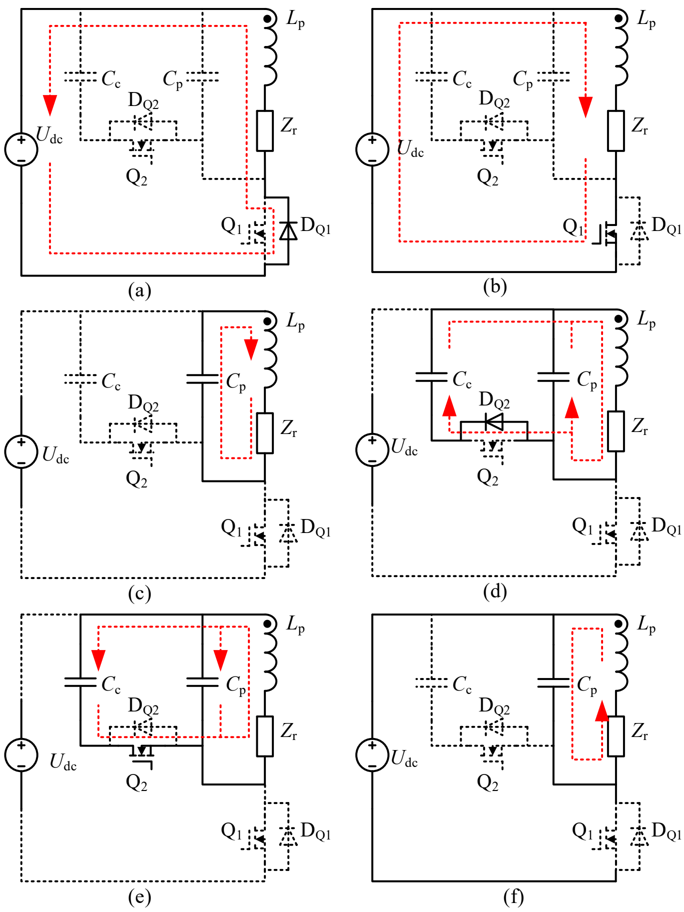

Figure 4. Operation process. (**a**) Mode 1 [t_0 ~ t_1]. (**b**) Mode 2 [t_1 ~ t_2]. (**c**) Mode 3 [t_2 ~ t_3]. (**d**) Mode 4 [t_3 ~ t_4]. (**e**) Mode 5 [t_4 ~ t_5]. (**f**) Mode 6 [t_5 ~ t_6].

Mode 3 [t_2 ~ t_3]: In Mode 3, all switches and diodes are turned off and the primary-side compensation capacitor C_p resonates with the transmitter coil L_p. Due to the fact that the period of this mode is very short, the value of i_{Lp} is approximately invariant, and the voltage of C_p decreases to zero and increases in reverse in this mode.

Mode 4 [t_3 ~ t_4]: In Mode 3, the voltage of C_p is reverse-charged to u_{Cc} (t_5). In time t_3, the body diode of the auxiliary switch Q_2 is turned on, providing a current path for i_{Lp} and enabling the auxiliary switch Q2 to achieve ZVS. In this mode, C_c is parallel to C_p and then resonates with L_p. C_c will acquire the maximum voltage in one operation period, and the voltage stress on the main switch can be computed as in (13). In time t_4, current i_{Lp} decreases to zero, which is the time to turn on the auxiliary switch Q_2.

Mode 5 [t_4 ~ t_5]: In time t_4, the auxiliary switch Q_2 is turned on. In this mode, L_p is charged by C_c and C_p, and the current i_{Lp} increases in reverse. In time t_5, the current i_{Lp} increases to the reverse maximum.

Mode 6 [$t_5 \sim t_6$]: In time t_5, the auxiliary switch Q_2 is turned off, and the primary-side compensation capacitor C_p resonates with the transmitting coil L_p. Due to the fact that the period of this operation mode is very short, the value of i_{Lp} is approximately invariant, and the voltage of C_p decreases to zero in reverse and increases to U_{dc} in positive at time t_6, and then Mode 6 ends and starts with Mode 1.

3. Switch Voltage Stress and Parameter Design

The operating process of the circuit is derived and the expression of the switch voltage stress is given to provide a basis for the circuit parameter design of the pull-up active-clamping wireless charging system.

In order to analyze and design the pull-up active-clamping wireless charging system proposed in this paper, the equivalent model when the main switch Q_1 is on or the auxiliary switch Q_2 is on is presented in Figure 5, where Z_r is the impedance of the receiving circuit, Z_{in} and Z_c are the input impedances of the transmitting circuit when the main switch Q_1 is turn on or the auxiliary switch Q_2 is turn on, r_p is the resistance of the L_p, and C_p is the primary compensation capacitor.

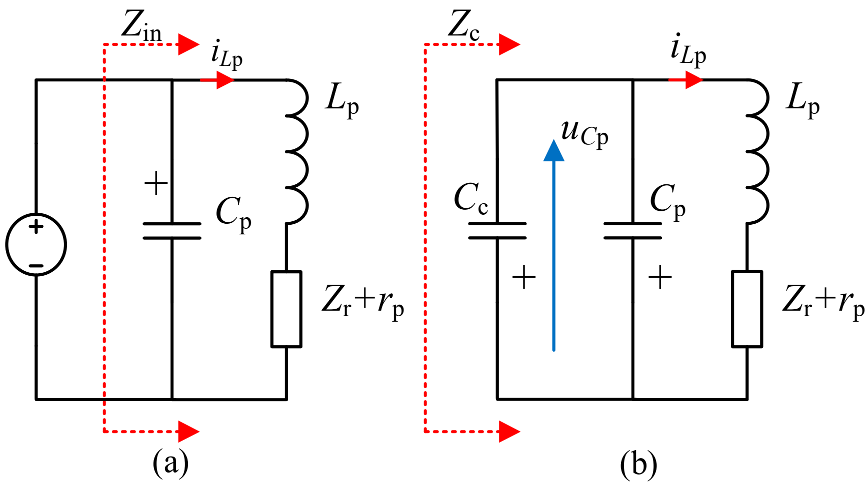

Figure 5. The equivalent model of the pull-up active-clamping wireless charging circuit. (**a**) Main switch Q_1 is turned on. (**b**) Auxiliary switch Q_2 is turned on.

The equations of the state when the main switch is turned on can be listed as follows. The positive direction coincides with the marks drawn in Figure 5a.

$$U_{dc} = i_{Lp}(t)(Z_r + r_p) + L_p \frac{di_{Lp}(t)}{dt} \tag{1}$$

where $i_{Lp}(t)$ is the instantaneous current value of the transmitter coil, the result is written as (2), where the range of t is $0 \sim DT$.

$$i_{Lp}(t) = \frac{U_{dc}}{Z_r + r_p}(1 - e^{-\frac{t}{\tau}}) \tag{2}$$

$$\tau = \frac{L_p}{Z_r + r_p} \tag{3}$$

By combining Formulas (2) and (3) in the moment the main switch is turned off, the value of $i_{Lp}(t)$ can be obtained:

$$I_{Lp} = \frac{U_{dc}}{Z_r + r_p}(1 - e^{\frac{-DT(Z_r + r_p)}{L_p}}) \tag{4}$$

where D is the duty cycle of the main switch and T is the time of one switching cycle.

Based on Figure 5b, the equation for the state when the auxiliary switch is turned on can be listed as follows:

$$\begin{cases} i_{L\mathrm{p}}(t) = (C_c + C_\mathrm{p})\frac{du_{C\mathrm{p}}(t)}{dt} \\ -u_{C\mathrm{p}}(t) = i_{L\mathrm{p}}(t)\cdot(Z_r + r_\mathrm{p}) + L_\mathrm{p}\frac{di_{L\mathrm{p}}(t)}{dt} \end{cases} \tag{5}$$

where $u_{C\mathrm{p}}(t)$ is the instantaneous voltage value of the resonant capacitor C_p, and the positive direction is shown in Figure 5b. The minus of the secondary formula of (5) indicates that the actual direction of the current passing through the inductor L_p is the opposite of the direction marked in Figure 5b during this period. Because of the discriminant function of (5):

$$\frac{(Z_\mathrm{r} + r_\mathrm{p})^2(C_\mathrm{p} + C_\mathrm{c}) - 4L_\mathrm{p}}{4L_\mathrm{p}^2(C_\mathrm{p} + C_\mathrm{c})} < 0$$

According to (5), $i_{L\mathrm{p}}(t)$ can be obtained:

$$i_{L\mathrm{p}}(t) = Ae^{\alpha t}\cdot\sin(\beta t + \varphi) \tag{6}$$

$$\begin{cases} \alpha = -\frac{Z_r + r_p}{2L_p} \\ \beta = \sqrt{\frac{4L_p - (Z_r + r_p)^2\cdot(C_p + C_c)}{4L_p^2(C_p + C_c)}} \end{cases} \tag{7}$$

When parameter t in function (6) is equal to zero, that means the auxiliary switch has just been turned on. The value of $i_{L\mathrm{p}}(t)$ and the differential of $i_{L\mathrm{p}}(t)$ can be computed as follows:

$$\begin{cases} I_{L\mathrm{p}} = A\sin\varphi \\ \left.\frac{di_{L\mathrm{p}}(t)}{dt}\right|_{t=0} = A\alpha\sin\varphi + A\beta\cos\varphi \end{cases} \tag{8}$$

From the above analysis, it is easy to conclude that the value of $I_{L\mathrm{p}}$ in Formula (8) is equal to the value in Formula (4). By combining Formulas (1), (5) and (8), the voltage instantaneous value of $u_{C\mathrm{p}}(t)$ can finally be computed as:

$$u_{C\mathrm{p}}(t) = A(Z_\mathrm{r} + r_\mathrm{p})e^{\alpha t}\sin(\beta t + \varphi) + L_\mathrm{p}\left[A\alpha e^{\alpha t}\sin(\beta t + \varphi) + A\beta e^{\alpha t}\cos(\beta t + \varphi)\right] \tag{9}$$

The equation can be rewritten to a conventional form as follows:

$$u_{C\mathrm{p}}(t) = Ae^{\alpha t}\sqrt{(Z_r + r_\mathrm{p} + \alpha)^2 + \beta^2 {L_\mathrm{p}}^2}\sin(t + \varphi + \gamma) \tag{10}$$

where the coefficients A, φ, and γ can be computed as follows from Formulas (1), (8) and (9):

$$\begin{cases} A = \sqrt{\left[\frac{U_\mathrm{dc} - I_{L\mathrm{p}}(Z_\mathrm{r} + r_\mathrm{p} + \alpha L_\mathrm{p})}{\beta L_p}\right]^2 + I_{L\mathrm{p}}^2} \\ \varphi = \arctan\left[\frac{I_{L\mathrm{p}}\beta L_\mathrm{p}}{U_\mathrm{dc} - I_{L\mathrm{p}}(Z_r + r_\mathrm{p} + \alpha L_\mathrm{p})}\right] \\ \gamma = \arctan(\frac{\beta L_\mathrm{p}}{Z_\mathrm{r} + r_\mathrm{p} + \alpha L_\mathrm{p}}) \end{cases} \tag{11}$$

Due to the resonance of capacitor C_p and inductor L_p on the primary side when the main switch is turned off, the voltage value of C_p will reach the maximum at the moment of the current value of $i_{L\mathrm{p}}(t)$ convert from positive to negative. From (6) and (10), the maximum voltage of C_p can be computed as follows:

$$u_{C\mathrm{pmax}} = A\beta L_\mathrm{p}e^{\alpha\frac{\pi - \varphi}{\beta}} \tag{12}$$

Based on (12), the voltage stress of the main switch can be computed:

$$u_{Q1\max} = U_{dc} + A\beta L_p e^{\alpha \frac{\pi-\varphi}{\beta}} \tag{13}$$

According to (7), if the clamp capacitor is large enough, the value of β does not change a lot with the variation of the clamping capacitor so that the value of (13) can be considered as a constant. The values of C_s and L_s do not influence the switch voltage stress, and only a small number of parameters need to be changed to adjust the switch voltage stress, which provides a convenient method to further introduce control strategies and improve system operation stability.

In addition, from the analysis of the working process and theoretical analysis in Figure 4, it can be seen that the maximum voltage of the clamp capacitor is the same as the maximum value of the primary-side compensation capacitor C_p, which can also be expressed as:

$$u_{Cc\max} = u_{Cp\max} = A\beta L_p e^{\alpha \frac{\pi-\varphi}{\beta}} \tag{14}$$

However, for a pull-down active-clamping circuit, the voltage of the clamp capacitor is the voltage of the primary-side compensation capacitor C_p plus the power source voltage, which is the voltage stress of the main switch. When the power source voltage is high, the voltage stress of the clamp capacitor will also be high, which is not conducive to capacitor selection. In addition, as the clamp capacitor C_c increases, the voltage stress difference between the main switch and the auxiliary switch becomes smaller, which means that within the same cycle, the clamp capacitor charges and discharges voltage less. Therefore, the voltage stress of the two switches can be changed by designing the value of the clamping capacitor C_c, in order to select a more suitable model and achieve the optimal cost.

The value of the compensation capacitor C_s can be calculated based on the theory of system total reactive power compensation, in which can achieve optimal system efficiency. The mathematical expression of which can be shown as follows:

$$\omega_0 L_s = \frac{1}{\omega_0 C_s} \tag{15}$$

where ω_0 is the operation angular frequency of this circuit.

The reflection impedance of the receiver also can be obtained:

$$Z_r = \frac{(\pi \omega_0 M)^2}{8R} \tag{16}$$

Defining Z_{in} as the total input impedance and L_p and Z_r + r_p as series firstly and then parallel to C_p, it can be calculated as shown:

$$Z_{in} = (Z_r + r_p + j\omega L_p)//\frac{1}{j\omega C_p} \tag{17}$$

To allow this system to completely implement reactive power compensation, the imaginary Z_{in} should equal zero, and C_p can be determined by:

$$C_p = \frac{L_p {R_{eq}}^2}{\omega_o^2 L_p^2 {R_{eq}}^2 + \left(\omega_o^2 M^2 + r_p R_{eq}\right)^2} \tag{18}$$

where R_{eq} is equal to 8 R/π^2. Generally, C_p should be less than this value to ensure weak inductance.

According to the above analysis, the whole parameter design method is as follows:

Firstly, the input voltage $U_{dc,}$ output voltage U_o, output current I_o, and frequency f are determined. Then, the inductance of L_p, L_s, and C_s is defined based on the voltage gain required for the wireless charging circuit. Next, the primary compensation capacitance C_p can be calculated with (18). Finally, the design of the clamp capacitor needs to take into account the switching voltage stress and soft switching. For the selection of parameters, the inductance of the transmitting and receiving coils determines the gain of the circuit. Generally speaking, the smaller the ratio of the inductance of the transmitting and receiving coils, the greater the gain. The mutual inductance determines the power level of the circuit. The primary-side compensation capacitor C_p determines the range of soft switching in the circuit. As the primary-side compensation capacitor C_p decreases, soft switching becomes easier to achieve. However, if it continues to decrease, there may be secondary resonance problems. Therefore, the value of C_p can be optimized based on the range of soft switching. The value of clamp capacitor C_c determines the voltage stress difference between two switches. The larger the value of clamp capacitor C_c, the smaller the voltage stress difference between the switches. Therefore, the selection of switch models and the price of switches under different voltage stresses can be comprehensively considered to optimize the value of clamp capacitor C_c. This is verified through the simulation in the next section.

The parameters of the pull-up active-clamping circuit can be determined using the above design method, as shown in Table 1.

Table 1. The parameters of the pull-up active-clamping circuit.

Symbol	Definition	Value
f	Frequency	1 MHz
U_{dc}	Input dc voltage	100 V
U_o	Output voltage	60 V
I_o	Output current	3 A
L_p	Transmitting coil inductance	5.5 µH
L_s	Receiving coil inductance	30 µH
M	Mutual inductance	3.5 µH
C_p	Primary-side compensation capacitor	220 pF
C_s	Secondary-side compensation capacitor	844 pF
C_c	Active-clamp capacitor	100 nF

4. Simulation and Experiment Results

According to the parameters shown in Table 1, the pull-up active-clamping circuit is simulated, as shown in Figure 6.

From Figure 6, it can be seen that the simulation waveform of the proposed pull-up active-clamping circuit is consistent with the analysis of the working process in Section 2. Both the main switch and auxiliary switch have achieved zero voltage turn-on, and the average voltage of the clamp capacitor C_c is around -143 V. In order to compare with the pull-down clamping circuit, a simulation was conducted on the pull-down clamping circuit under the same input and output, as well as coil and capacitor parameters. The waveform is shown in Figure 7.

As shown in Figure 7, with the same parameters, the pull-down active-clamping circuit is basically the same as the pull-up active-clamping circuit in terms of output voltage, switch voltage stress, and coil current. However, the average clamp capacitor voltage of the pull-down active-clamping circuit is about 245 V, which is larger than that of the pull-up active-clamping circuit.

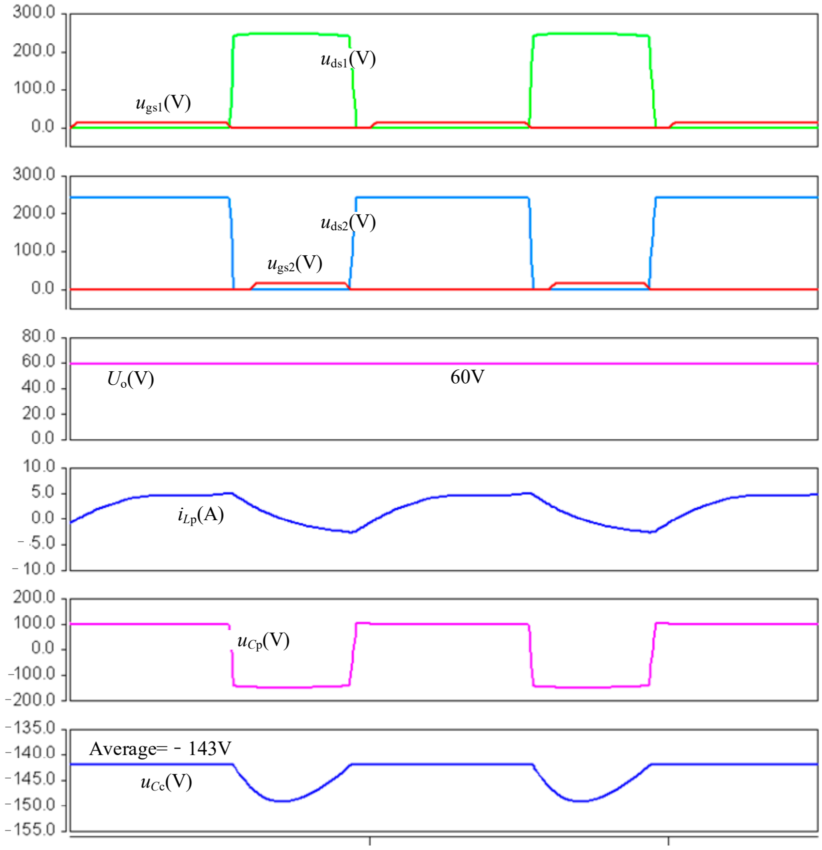

Figure 6. Simulation diagram of the proposed pull-up active-clamping circuit.

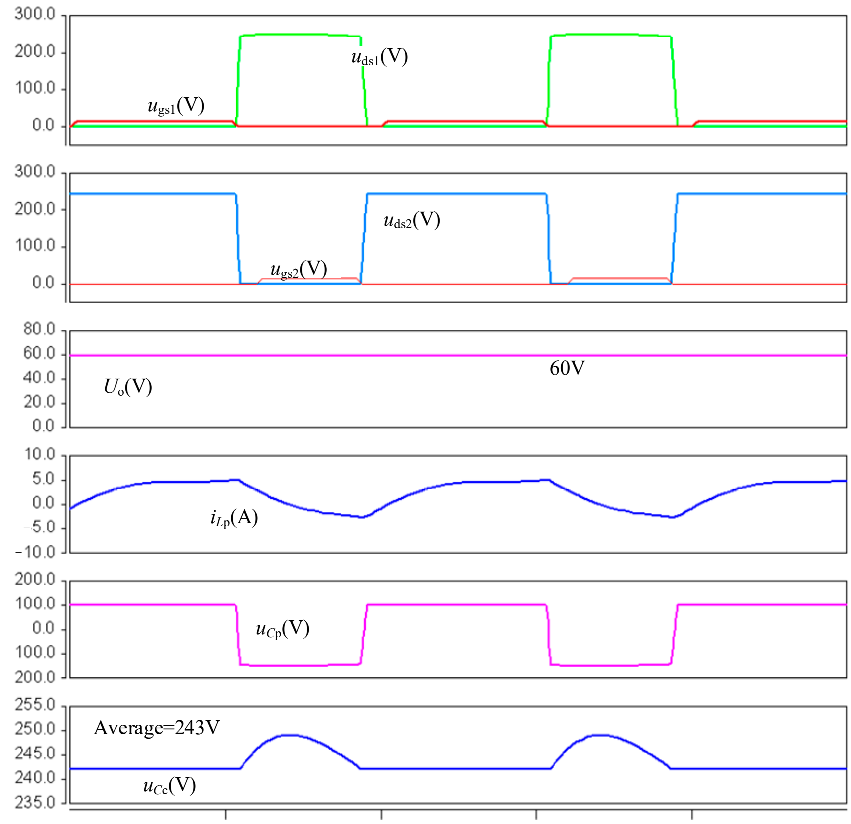

Figure 7. Simulation diagram of the pull-down active-clamping circuit.

For the proposed pull-up active-clamping circuit, the voltage stress curves of the main switch and auxiliary switch were simulated as the clamping capacitor C_c changed, as shown in Figure 8.

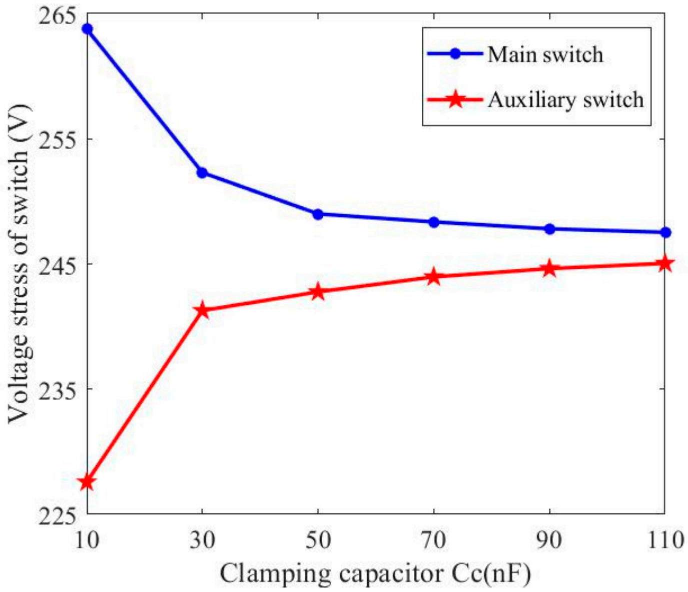

Figure 8. Switch voltage stress under changes in the clamping capacitor.

As can be seen in Figure 8, as the clamping capacitor C_c changes from 10 nF to 110 nF, the main switch voltage stress gradually decreases, the auxiliary switch voltage stress gradually increases, the rate of change becomes slower and slower, and the voltage stress of the main switch is always higher than that of the auxiliary switch. According to the results shown in Figure 8, the selection of switches can be comprehensively considered to optimize C_c so as to achieve the optimal cost for the capacitance of the two switches and C_c.

To validate the proposed circuit, a 1 MHz 180 W wireless charging system was built and is shown in Figure 9.

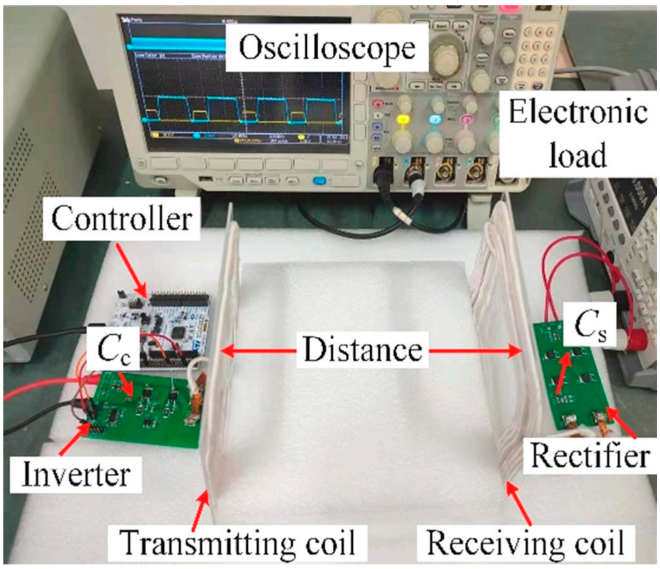

Figure 9. Experimental platform diagram of the proposed pull-up active-clamping circuit.

Figure 10 shows the ZVS waveforms of the main switch and the auxiliary switch in the pull-up active-clamping circuit. The duty cycle of the main switch is 0.5 and that of the auxiliary switch is 0.3. It can be seen from Figure 10 that the measured voltage stress of the main and auxiliary switch is 250 V and 245 V, respectively, which is close to the theoretical results. Compared with the traditional single-switch converter, e.g., Class E in [7], the voltage stress of the switch decreases by 30.6% at the same input voltage. In addition, the ZVS margin of the main switch and auxiliary switch is 45 ns and 60 ns, respectively, indicating the high reliability of the circuit proposed in this paper and the correctness of the proposed parameter design method.

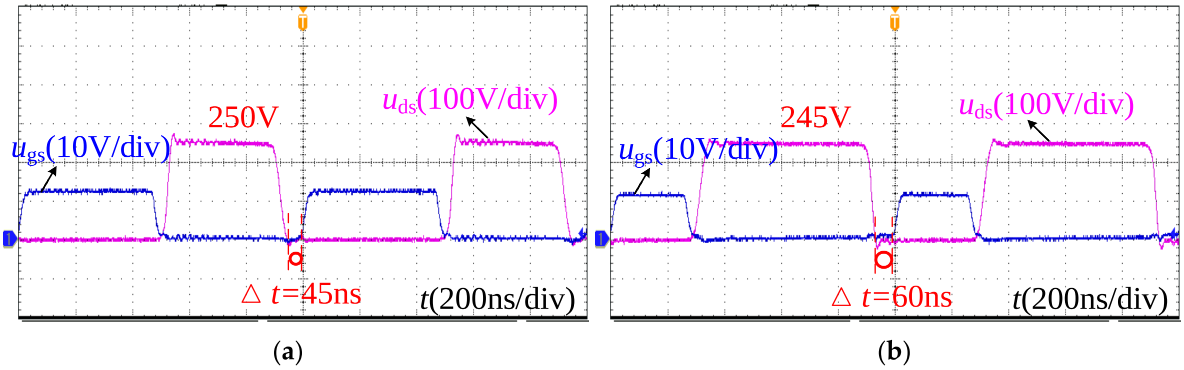

Figure 10. u_{gs} and u_{ds} waveforms of the active-clamping circuit. (**a**) Main switch. (**b**) Auxiliary switch.

The variation of system output power and efficiency (dc to dc) with load resistance is drawn in Figure 11. It can be seen from Figure 11 that the output power increases as the load increases from 11 Ω to 15 Ω, and the output power decreases as the load increases from 15 Ω to 30 Ω. The maximum efficiency is about 91%, and the efficiency is above 88.5% during the whole load change process.

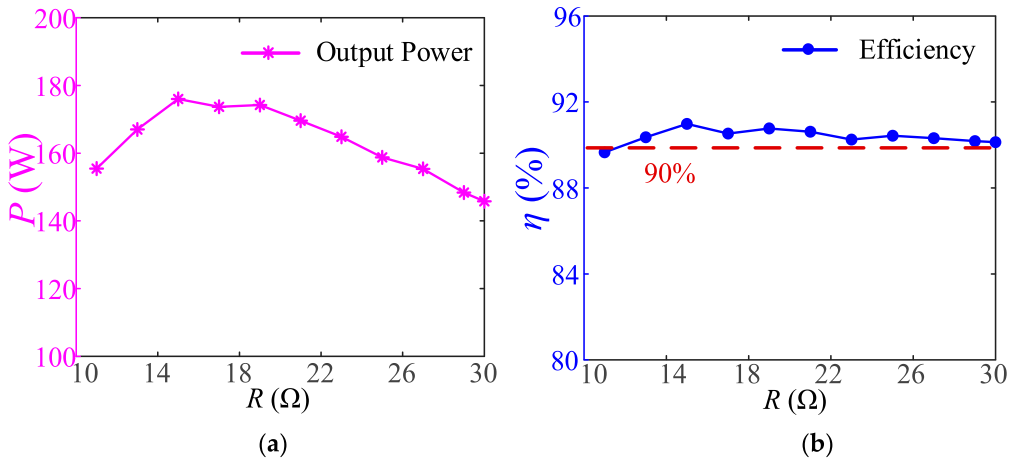

Figure 11. (**a**) The curve of output power. (**b**) The curve of efficiency.

The power loss of each part of the system is shown in Figure 12. As can be seen, the switch loss and coil loss account for 25% and 34% of the circuit loss, which is the majority of the loss. Therefore, the efficiency can be further improved by selecting a switch with lower on-resistance or by reducing the AC resistance of the coils.

A comparison of the cost and efficiency of the Class E circuit with the pull-up active-clamping circuit is shown in Table 2. It can be seen from Table 2 that, although the active-clamp topology adds a switch and a clamp capacitor, the efficiency is similar to that of the Class E circuit due to low voltage stress and low on-resistance. However, the Class E circuit requires an AC inductor—a high-frequency AC inductor costs $3.49—and the active-clamp circuit does not require additional inductance. Moreover, due to the larger switch capacity required for Class E circuits, the total cost of power switches required is approximately 38% higher than that of active-clamp circuits. Therefore, the active-clamping circuit has great advantages in switch costs. (The prices in the table are all on the website: https://activity.szlcsc.com/, accessed on 1 March 2023).

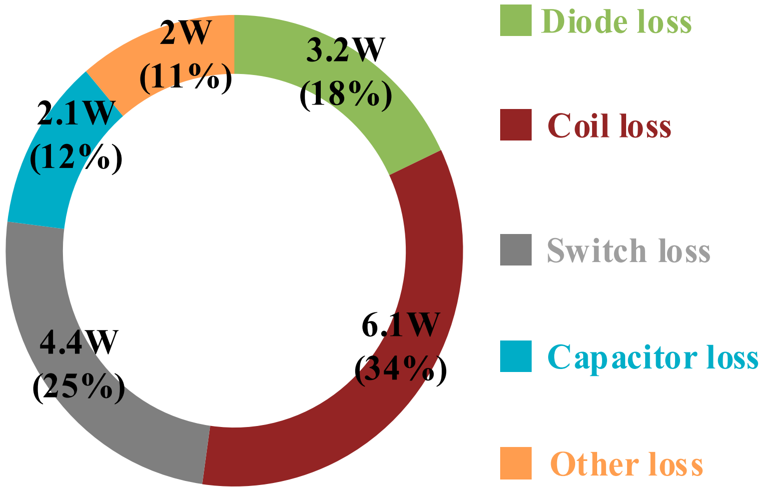

Figure 12. The losses of the pull-up active-clamping circuit.

Table 2. The comparison of two circuits in efficiency and switch cost.

	Active Clamp Circuit	Class E Circuit
Efficiency	91%	90.8%
Price of inductor	--	$3.49
Total switch price	$0.69	$1.12

The comparison between the proposed circuit and some wireless power transfer circuits on the number of devices, efficiency, and voltage stress ratio is given in Table 3. The voltage stress ratio is defined as the maximum voltage of the switch divided by the input voltage. As can be seen from Table 3, the pull-up active-clamping circuit does not require additional inductors compared to [7,8,11,12] and has less voltage stress compared to [10,11].

Table 3. Performance comparison of various topologies.

	Circuit	Frequency	Output Power	Voltage Stress Ratio	Number of Inductors	Efficiency
Proposed	Active clamp	1 MHz	180 W	2.3	0	91%
[7]	Class E	100 kHz	450 W	3.6	1	90.3%
[9]	Class EF	6.78 MHz	25 W	2.5	2	75%
[10]	Single-switch	100 kHz	180 W	4.8	0	90.5%
[11]	Class E^2	6.78 MHz	10 W	4.06	2	85%
[12]	Class ϕ_2	10 MHz	18 W	3	1	85.5%

5. Conclusions

In this paper, a pull-up active-clamping circuit is proposed for small- or medium-power wireless charging. A low-cost and compact-size wireless charging system can be achieved due to the low component count and low-voltage-stress switch of the proposed pull-up active-clamping circuit. The experimental results validate the zero voltage turn-on and low dv/dt operations over a wide load resistance range. A 30.6% switch voltage stress reduction and a 38% power switch cost reduction are achieved in the prototype system. In addition, compared to the pull-down clamp circuit, the clamp capacitor voltage of the pull-up clamp circuit is lower, which has a greater cost advantage.

Author Contributions: Writing—original draft, B.P.; resources and conceptualization, H.L.; writing—review and editing, Y.W.; project administration, D.Z. All authors have read and agreed to the published version of the manuscript.

Funding: This research received no external funding.

Data Availability Statement: Not applicable.

Conflicts of Interest: The authors declare no conflict of interest.

References

1. Aldhaher, S.; Yates, D.C.; Mitcheson, P.D. Load-Independent Class E/EF Inverters and Rectifiers for MHz-Switching Applications. *IEEE Trans. Power Electron.* **2018**, *33*, 8270–8287. [CrossRef]
2. Anurag, A.; Acharya, S.; Prabowo, Y.; Gohil, G.; Bhattacharya, S. Design Considerations and Development of an Innovative Gate Driver for Medium-Voltage Power Devices with High dv/dt. *IEEE Trans. Power Electron.* **2019**, *34*, 5256–5267. [CrossRef]
3. Li, H.; Liu, M.; Yang, Y.; Song, Z.; Wang, Y. A Multi-MHz Active Clamp Topology for High Cost-Performance Wireless Power Transfer. *IEEE Trans. Power Electron.* **2022**, *37*, 12828–12840. [CrossRef]
4. He, L.; Guo, D. Compound Voltage Clamped Class-E Converter with ZVS and Flexible Power Transfer for WPT System. *IEEE Trans. Power Electron.* **2020**, *35*, 7123–7133. [CrossRef]
5. Li, H.; Liu, M.; Kong, L.; Wang, Y. An Independent Dual-Coil Driving Topology for Wireless Power Transfer. *IEEE Trans. Power Electron.* **2023**, *38*, 1378–1383. [CrossRef]
6. Ke, G.; Chen, Q.; Zhang, S.; Xu, X.; Xu, L. A Single-Ended Hybrid Resonant Converter with High Misalignment Tolerance. *IEEE Trans. Power Electron.* **2022**, *37*, 12841–12852. [CrossRef]
7. Li, H.; Yang, Y.; Chen, J.; Xu, J.; Liu, M.; Wang, Y. A Hybrid Class-E Topology with Constant Current and Constant Voltage Output for Light EVs Wireless Charging Application. *IEEE Trans. Transp. Electrif.* **2021**, *7*, 2168–2180. [CrossRef]
8. Pan, B.; Li, H.; Wang, Y.; Li, J. A Switched Capacitor-Based Single Switch Circuit with Load-Independent Output for Wireless Power Transfer. *Electronics* **2022**, *11*, 1400. [CrossRef]
9. Aldhaher, S.; Yates, D.C.; Mitcheson, P.D. Design and Development of a Class EF2 Inverter and Rectifier for Multimegahertz Wireless Power Transfer Systems. *IEEE Trans. Power Electron.* **2016**, *31*, 8138–8150. [CrossRef]
10. Yue, R.; Wang, C.; Li, H.; Liu, Y. Constant-Voltage and Constant-Current Output Using P-CLCL Compensation Circuit for Single-Switch Inductive Power Transfer. *IEEE Trans. Power Electron.* **2021**, *36*, 5181–5190. [CrossRef]
11. Song, J.; Liu, M.; Ma, C. Analysis and Design of a High-Efficiency 6.78-MHz Wireless Power Transfer System with Scalable Number of Receivers. *IEEE Trans. Ind. Electron.* **2020**, *67*, 8281–8291. [CrossRef]
12. Zhang, Z.; Zou, X.; Dong, Z.; Zhou, Y.; Ren, X. A 10-MHz eGaN Isolated Class-Φ2 DCX. *IEEE Trans. Power Electron.* **2017**, *32*, 2029–2040. [CrossRef]